

Structures for Organic Diode Lasers and Optical Properties of Organic Semiconductors Under Intense Optical and Electrical Excitations

V. G. Kozlov, G. Parthasarathy, Paul E. Burrows, V. B. Khalfin, J. Wang, S. Y. Chou, and S. R. Forrest

Invited Paper

Abstract—The challenges to realizing diode lasers based on thin films of organic semiconductors are primarily related to low charge carrier mobility in these materials. This not only limits the thickness of organic films to ≤ 100 nm in electrically pumped devices, but it also leads to changes in the optical properties of organic films induced by the large number of carriers trapped in the materials subjected to an intense electrical excitation. We describe organic waveguide laser structures composed of thin organic films and transparent indium–tin–oxide electrodes. These waveguides allow for efficient injection of an electrical current into the organic layers and provide for low optical losses required in a laser. The changes in the optical properties of organic thin films induced by electrical excitation are studied using electroluminescence and pump and probe spectroscopy. Induced transparency and absorption observed in the organic materials may be related to triplet excitons or trapped charge carriers. Pump-induced absorption is also observed in organic films under quasi-CW optical excitation. These effects must be taken into account both in the design of organic diode laser structures and in the selection of charge transporting materials.

I. INTRODUCTION

ORGANIC lasers were demonstrated in the late 1960's employing organic molecules in liquid solutions [1], [2] or as dopants in solids or thin films [2], [3], including organic crystals [4], [5]. In all of these lasers, optical excitation has been used to deliver energy to the light-emitting molecules. Recently, lasing has been observed in optically pumped thin films of conjugated polymers [6]–[9] and small molecular weight organic semiconductors doped with dye molecules [10], [11] also used in efficient organic light-emitting devices (OLED's), where the excitation is delivered to the light-emitting species by an electric current. These experiments initiated work on electrically pumped organic semiconductor lasers (OSL's) which, compared to conventional laser diodes, should have advantages in applications such as optical sensing and communications [12], [13].

It has also been shown that lasing thresholds can be substantially decreased if nonradiative Forster energy transfer

Manuscript received May 25, 1999. This work was supported in part by DARPA, the Air Force Office of Scientific Research, the National Science Foundation Materials Research Science and Engineering Center, and Universal Display Corporation.

The authors are with the Center for Photonics and Optoelectronic Materials (POEM), Department of Electrical Engineering and the Princeton Materials Institute, Princeton University, Princeton NJ 08544 USA.

Publisher Item Identifier S 0018-9197(00)00304-3.

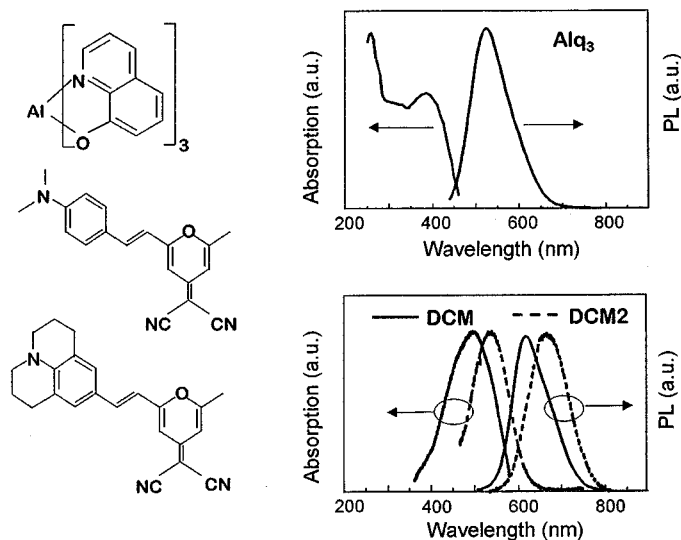


Fig. 1. Left column: chemical structure formulas of Alq₃, DCM and DCM2, respectively. Right column: absorption and PL spectra of Alq₃, DCM, and DCM2.

[14] is employed to deliver the excitation to the light-emitting molecules, or lumophores [5], [10], [11]. A thin film of tris-(8-hydroxyquinoline) aluminum (Alq₃) [Fig. 1(a)], doped with 1–5% of DCM [see Fig. 1(b)] or DCM2 [Fig. 1(c)] laser dye molecules, provides an example of one such energy transfer system. The overlap between the Alq₃ photoluminescence (PL) and DCM absorption spectra [Fig. 1(d) and (e)] leads to efficient energy transfer of excitation from Alq₃ to DCM [15]. As a result, the absorption band of the Alq₃:DCM film is separated from the emission spectral band, leading to very low lasing thresholds in these materials [16]. Excitation of lumophores by means of Forster energy transfer also improves operational lifetimes of optically pumped OSL's [15].

Alq₃:DCM films are also employed as light-emitting materials in efficient OLED's [17]. The intensity of electrical excitation achieved in these devices is comparable to the optical pump energy required for lasing [18]. However, there are two major issues that have to be resolved before electrically pumped OSL's can be demonstrated. First, it has to be shown that electrical excitation leads to optical gain in organic films. Second, low-loss laser structures composed of thin organic films combined with

contact electrodes have to be demonstrated. In this paper, we address both of these issues and discuss the prospects for eventually realizing electrically pumped OSL's.

II. LASING IN OPTICALLY PUMPED ORGANIC FILMS

The study of lasing in optically pumped organic films provides a guideline to the design of electrically pumped OSL's. Characteristics of optically pumped lasers such as lasing thresholds, quantum efficiency, spectral tunability, and linewidth of emission may be used to predict properties of electrically pumped devices and evaluate their potential for industrial applications [12], [13]. It is also feasible that optically pumped organic lasers employing compact pump sources, such as GaN diode lasers, might find practical applications.

Lasing in optically pumped organic thin films has been demonstrated employing a variety of optical resonators, including organic waveguides [10], planar microcavities [13], microdisks [19], microrings [20], and even two-dimensional (2-D) distributed feedback (DFB) structures [21]. Among all of these structures, waveguide lasers provide for the lowest lasing thresholds, which is an essential aspect in the design of electrically pumped OSL's. We have demonstrated recently how lasing thresholds of electrically pumped OSL's may be estimated from characteristics of optically pumped waveguide OSL's composed of an organic double heterostructure [10]. Here, we study optically pumped double-heterostructure OSL's with distributed optical feedback, employing a first-order optical grating fabricated by nanoimprint technology.

An Alq₃:DCM double heterostructure, shown schematically in the inset of Fig. 2(a), consists of a 50-nm-thick layer of Alq₃ doped with 2% of DCM, sandwiched between two 125-nm-thick cladding layers of Alq₃. The organic layers were fabricated by sublimation in vacuum (5×10^{-7} torr) on a Si substrate precoated with a 1.8- μm -thick layer of SiO₂. The organic film (Alq₃ refractive index $n = 1.72$) forms an optical waveguide with SiO₂ ($n = 1.46$) and air ($n = 1$) used as cladding layers. In this structure, the Alq₃:DCM active layer is placed at the maximum of the optical field intensity in the waveguide, resulting in an optical confinement factor of $\Gamma=18\%$ [15], which is enhanced by a higher refractive index of Alq₃:DCM ($n = 1.78$).

Optical feedback is provided by a grating (200-nm period, 30-nm depth) etched in the SiO₂ cladding prior to deposition of the organic film. The etching is accomplished using nanoimprint lithography, a high-throughput and low-cost patterning method with a sub-10-nm resolution [22], [23]. In the nanoimprint lithography process, a 200-nm period grating mold was first fabricated by interference lithography. The grating pattern was imprinted into a layer of polymethylmethacrylate (PMMA) spun on the SiO₂-Si substrate. Before imprinting, both the mold and the PMMA-coated substrate were heated to 175 °C, where the polymer is a viscous fluid. The mold was then pressed at approximately 600 psi into the PMMA to create a thickness contrast pattern in the polymer. After cooling, the mold was separated from the substrate. The thin residual resist in the recessed region was removed by oxygen reactive ion

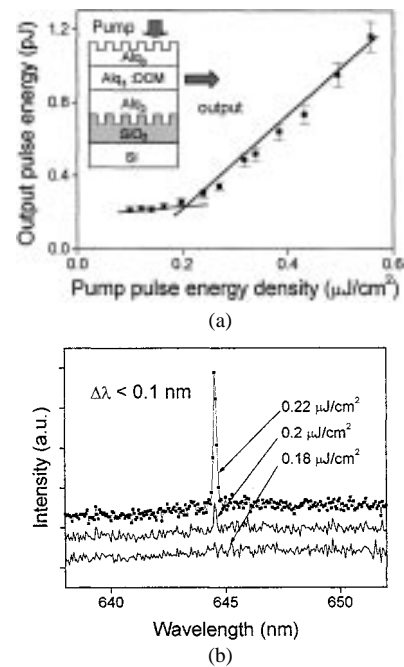


Fig. 2. (a) Dependence of output energy on the input pump energy near threshold for a Alq₃:DCM DFB laser (solid lines are fits to the experimental points). Inset: schematic diagram of Alq₃:DCM double-heterostructure DFB laser. (b) Emission spectra of Alq₃/DCM double-heterostructure DFB laser at increasing excitation levels near threshold.

etching. The pattern was transferred into SiO₂ by evaporation of a thin Cr layer, followed by lift-off, and finally reactive ion etching of SiO₂ with CHF₃ [22], [23].

The laser structure was optically pumped with 1-ns pulses generated at a 40-Hz repetition rate by a nitrogen laser at wavelength $\lambda=337$ nm, focusing the pump laser beam into a $2 \text{ cm} \times 50 \mu\text{m}$ stripe on the device surface. The stripe was oriented orthogonal to the grating to couple the reflection back into the pumped region of the device. Lasing action associated with a sharp increase in output power [Fig. 2(a)] and spectral narrowing [Fig. 2(b)] was observed at a pump energy density above $0.2 \mu\text{J}/\text{cm}^2$, accounting for 10% of the incident laser power absorbed in the active region (Alq₃ absorption is $\alpha=3 \times 10^4 \text{ cm}^{-1}$ at $\lambda=337$ nm [24]). The experiments were conducted in a nitrogen ambient and no degradation in the performance of the devices was observed during several hours of operation.

The lasing thresholds observed in double-heterostructure DFB OSL's ($P_{\text{th}} = 0.2 \mu\text{J}/\text{cm}^2$) are significantly lower than thresholds of Fabry-Perot double-heterostructure OSL's ($P_{\text{th}} = 1 \mu\text{J}/\text{cm}^2$) [10], where optical feedback is provided by reflections from the organic film facets. Low reflectivity of the facets ($R = 7\%$) leads to relatively high optical losses in Fabry-Perot double-heterostructure OSL's, resulting in higher lasing thresholds. The DFB structures provide for efficient optical feedback, and the optical losses are limited only by waveguide and scattering losses from grating imperfections. While it is not possible to quantify all of these effects, we can conclude that optical gain is significant in Alq₃:DCM films under an optical excitation intensity $<0.2 \mu\text{J}/\text{cm}^2$.

These experiments provide an estimate for lasing thresholds in electrically pumped OSL's. An optical energy density of

$P_{\text{th}} = 0.2 \mu\text{J}/\text{cm}^2$, absorbed in the $\text{Alq}_3:\text{DCM}$ layer, corresponds to a density of $3 \times 10^{11} \text{ cm}^{-2}$ photons. This leads to $n = 3 \times 10^{11} \text{ cm}^{-2}$ excitons formed in the $\text{Alq}_3:\text{DCM}$. An equivalent density of excitons may be formed by an injection current of $j = 80 \text{ A}/\text{cm}^2$, estimated using the equation

$$j = \frac{2 \cdot n \cdot e}{\chi \cdot \tau} \quad (1)$$

where e is the electron charge, $\tau = 5 \text{ ns}$ is the DCM radiative lifetime [25], $\chi = 1/4$ is the ratio of radiative singlet excitons to the total number of excitons formed by electrical injection, and the factor of 2 accounts for two charges (electron and hole) needed to form an exciton. This level of injection is easily achieved in OLED's, as discussed in Section IV, opening up the realistic possibility for achieving electrically pumped OSL's.

III. OPTICAL PROPERTIES OF ORGANIC LASER MATERIALS UNDER QUASI-CW OPTICAL EXCITATION

All organic thin-film lasers demonstrated so far employed pulsed ($t = 100 \text{ fs}$ – 10 ns) optical excitation as a pump. Pulsed pump sources such as a nitrogen laser or a frequency-tripled YAG laser provide pulses of ultraviolet (UV) radiation ($\lambda \approx 350 \text{ nm}$) with energies in excess of the lasing thresholds in the organic thin films. However, the low optical intensities required to achieve lasing in $\text{Alq}_3:\text{DCM}$ DFB OSL's may also be obtained using CW UV sources such as an Ar-ion laser, opening the possibility to observe lasing under continuous, or quasi-continuous, optical excitation.

For experiments focused on determining the quasi-CW lasing characteristics of organic films, we fabricated DFB OSL structures consisting of a single 300-nm-thick Alq_3 layer doped with 2% DCM, shown schematically in the inset of Fig. 3. These devices provide for the lowest lasing threshold in terms of total incident pump intensity $P_{\text{th}} = 1.5 \text{ kW}/\text{cm}^2$, while double-heterostructure DFB OSL's (discussed above) have the lowest threshold in terms of pump energy absorbed in the active layer. Pump intensities $>1.5 \text{ kW}/\text{cm}^2$ were achieved using a 2.5-W CW Ar-ion laser ($\lambda = 351$ – 363 nm), focusing the laser beam into a $5 \text{ mm} \times 20 \mu\text{m}$ stripe. To reduce the degradation of the organic film under high-intensity excitation, the experiments were conducted in nitrogen ambient, and the CW pump laser was modulated with a mechanical chopper, resulting in a 0.2-ms-long pump laser pulses at 40-Hz repetition rate. However, no lasing action was observed under such excitation.

To further examine the effect of CW excitation, we combined pulsed (1 ns) and quasi-CW (0.2 ms) excitations focusing both the nitrogen and Ar-ion laser beams onto the same region of the organic film. The intensity of the pulsed excitation was tuned above the lasing threshold, and the DFB laser output power was monitored as a function of time delay between the 1- and 0.2-ms excitation pulses (Fig. 3). We found that the laser output power decreases by 30% once the pulse overlaps the quasi-CW excitation. The laser output power slowly recovers as the pulsed excitation is further delayed behind the quasi-CW pulse. The measurements presented in Fig. 3 were also affected by a gradual degradation of the organic film during the experiments, resulting in a difference between the laser output power at time delay

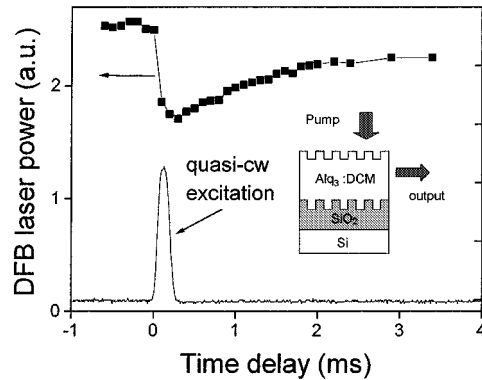


Fig. 3. Output power of $\text{Alq}_3:\text{DCM}$ DH DFB laser as a function of time delay between pulsed and quasi-CW pump pulses. Intensity profile of the quasi-CW excitation is also shown in the lower part of the graph.

$t = -0.5 \text{ ms}$, measured at the beginning of the experiments, and the power at $t = 3.5 \text{ ms}$.

To exclude sample heating as the origin of the observed decrease in the laser output, we also fabricated laser structures on a thermally insulating glass substrate. The temperature change in a 300-nm-thick organic film is primarily determined by the thermal conductivity of the underlying substrate. Hence the heating of an optically pumped organic film fabricated on a Si substrate (thermal conductivity $\kappa = 150 \text{ W}/\text{m}\cdot\text{K}$) is expected to be smaller than heating of a film fabricated on glass ($\kappa = 1.1 \text{ W}/\text{m}\cdot\text{K}$), since the film temperature change $\Delta T \sim E/(\kappa t)^{-1/2}$ [26], where E is the pump pulse energy and t is time after the excitation. The thermal time constant should also be different in laser structures fabricated on Si and glass. We found, however, that the effect of quasi-CW excitation on lasing has the same amplitude and time constant in the lasers fabricated on glass and Si, indicating that sample heating is not responsible for the observed decrease in the laser output power.

These data suggest that the quasi-CW excitation induces additional optical losses in the organic film. To further understand the origin of the effect, we used a pump and probe configuration, where 0.2-ms duration pump pulses were provided by the modulated output of a cw Ar-ion laser ($\lambda = 351$ – 363 nm), and the probe was supplied by a CW diode laser ($\lambda = 675 \text{ nm}$). The experiments were conducted with a 300-nm-thick Alq_3 film doped with 2% of DCM on a quartz substrate. The pump ($P = 10$ – 100 mW) and probe ($P = 0.1 \text{ mW}$) beams were focused into a 1-mm-diameter spot on the $\text{Alq}_3:\text{DCM}$ film. The intensity of the probe beam was analyzed using a balanced detector combined with a digital oscilloscope. To avoid detection of photoluminescence generated by the pump, the collimated probe beam was passed through a 1-mm-diameter diaphragm placed 0.7 m away from the sample. The experiments were conducted in nitrogen ambient to reduce photochemical degradation of the organic film.

The results of the pump-probe experiments, shown in Fig. 4, offer a clear indication of absorption induced by the quasi-CW optical excitation. The changes measured in the probe laser intensity transmitted through a 300-nm-thick $\text{Alq}_3:\text{DCM}$ film [Fig. 4(b)] are correlated with the pump pulse [Fig. 4(a)]. The induced absorption has a 10–50- μs rise time following the front edge of the pump pulse and has a decay time of $t = 0.16 \text{ ms}$.

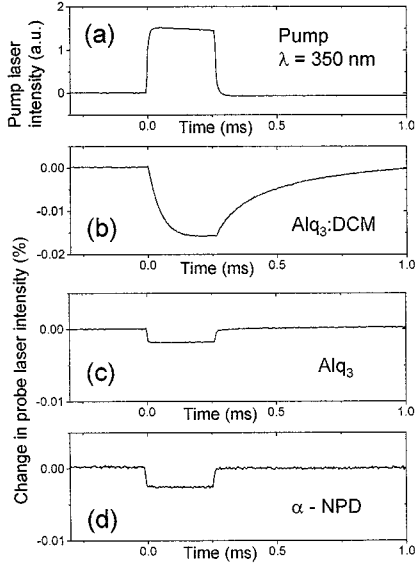


Fig. 4. (a) Optical pump ($\lambda=350\text{--}360$ nm) pulse and (b) pump-induced absorption measured at $\lambda=650$ nm in a 300-nm-thick Alq_3 film doped with 2% of DCM. Also, pump-induced absorption for (c) Alq_3 and (d) $\alpha\text{-NPD}$ are shown.

The amplitude of the induced absorption increases linearly over a limited range of pump power density ($P = 1\text{--}10$ W/cm^2). The measurements are limited by the system sensitivity at low excitation powers, and by the pump-induced photoluminescence at $P > 10$ W/cm^2 . Similar effects were observed in 300-nm-thick films of undoped Alq_3 [Fig. 4(c)], and in a 200-nm-thick film of $\alpha\text{-NPD}$ [Fig. 4(d)], where the induced absorption has a smaller amplitude and shorter rise and decay times. This suggests that the pump-induced absorption observed in $\text{Alq}_3:\text{DCM}$ is primarily due to the dopant molecules.

It is well known that the performance of CW lasers utilizing liquid solutions of dye molecules is strongly affected by absorption of triplet excitons formed from singlet excitons by intersystem crossing on a timescale of 100 ns, and possessing millisecond radiative decay times [27] and [28]. Similar processes might take place in the $\text{Alq}_3:\text{DCM}$ film subjected to quasi-CW optical excitation. Alternatively, excitons formed in the film may dissociate into single charge excitations, or polarons. The optical properties of a molecular ion possessing an extra electron (or hole) are expected to be different from those of a neutral molecule. The presence of an extra charge changes the energy of molecular excitations and creates new electronic transitions. Induced absorption was also observed in the $\text{Alq}_3:\text{DCM}$, Alq_3 , and $\alpha\text{-NPD}$ films subjected to intense electrical excitation, as discussed in Section V. These effects have direct implications on the realization of electrically pumped OSL's, as discussed below.

IV. ORGANIC LASER DIODE STRUCTURES

There are two essential requirements in the design of an organic laser diode. First of all, it has to provide for efficient current injection in the optically active material (such as $\text{Alq}_3:\text{DCM}$), and second, it has to form an optical resonator, whose optical losses are smaller than the gain. The challenges

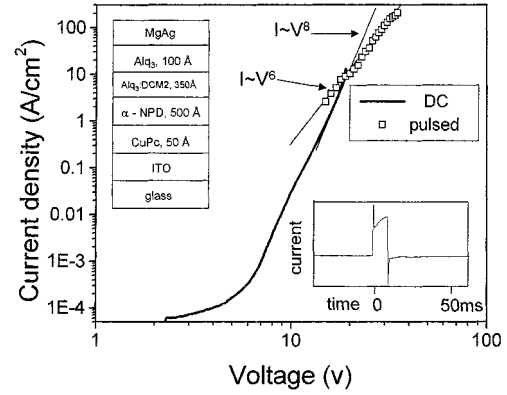


Fig. 5. Current–voltage characteristic of an OLED under dc and pulsed excitation. Top inset: the OLED structure. Bottom inset: current in the OLED as a function of time.

in realizing such structures are primarily related to the intrinsically low charge carrier mobilities in organic semiconductors.

Charge transport in small molecular weight organic semiconductors, such as Alq_3 , is usually described in terms of trap-charge-limited current [24]

$$J \approx \mu(E, T) \cdot \frac{V^{(m+1)}}{d^{(2m+1)}} \quad (2)$$

where

$\mu(E, T)$ charge carrier mobility at electric field E and temperature T ;

V applied voltage;

d organic film thickness.

Here $m = T_t/T$, where T_t is the characteristic temperature of the trap distribution. The carrier mobility in molecular semiconductors is a strong function of the applied electric field and injected carrier density [24]. Carrier injection in Alq_3 raises the electron quasi-Fermi level toward the lowest unoccupied molecular orbital (LUMO), reducing the available density of empty traps and increasing the electron effective mobility. This dependence may be taken into account by varying the m value [see (2)] at increasing injection levels. For example, the charge transport in Alq_3 is adequately described by (2) with $\mu_n = (5 \pm 2) \times 10^{-5}$ $\text{cm}^2/\text{V}\cdot\text{s}$, and m ranging from 1 at low applied voltages to 8 at high voltages [24].

To determine charge transport mechanisms under intense electrical excitation, we fabricated OLED's composed of a 50-Å-thick film of copper phthalocyanine (CuPc), 500 Å of 4, 4'-bis[N -(1-naphthyl)- N -phenyl-amino] biphenyl ($\alpha\text{-NPD}$), 350 Å of $\text{Alq}_3:\text{DCM2}$ (doped with 3% of DCM2 by mass), and 100 Å of Alq_3 (see Fig. 5, inset). The organic layers were grown in vacuum (5×10^{-7} torr) on a prepatterned indium–tin-oxide (ITO) coated glass substrates. A 1000-Å-thick layer of Mg:Ag (10:1) was used as the cathode. The OLED's were encapsulated in an argon ambient [29] prior to characterization in order to minimize degradation of the organic layers.

Fig. 5 shows the current versus voltage characteristics of an OLED measured under dc and pulsed (10 μs) excitation. A maximum current density of $j = 300$ A/cm^2 was attained under pulsed excitation. This demonstrates that excitation intensities

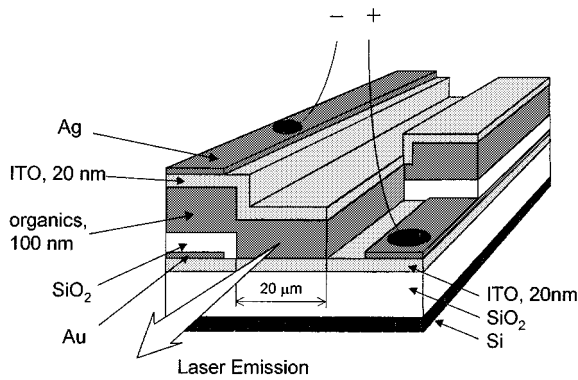


Fig. 6. Schematic of a waveguide OLED composed of a 100-nm-thick organic film and 20-nm-thick ITO contacts.

in excess of those required for lasing in optically pumped structures can be achieved. The different slopes of I - V characteristics measured under dc ($I \sim V^8$) and pulsed ($I \sim V^6$) conditions may be explained in terms of trap-charge-limited conductivity in these materials [24]. The reduction in m implies a smaller characteristic energy of traps ($m = E_t/kT$, where E_t is the characteristic trap energy and k is Boltzmann's constant) contributing to charge transport under pulsed ($\tau=10 \mu\text{s}$) excitation, suggesting the presence of deep electronic states with charge hopping times in excess of $10 \mu\text{s}$. This can also be inferred from the electrical current pulse profile, shown in Fig. 5, bottom inset, where the current slowly increases in response to a $10\text{-}\mu\text{s}$ voltage pulse.

The low charge carrier mobility combined with a strong dependence of trap-charge-limited currents on the film thickness [see (2)] imposes strict limitations on the thickness of organic layers employed in OSL's. In most OLED's, the total thickness of organic layers is typically from 100 to 150 nm, with current injection becoming increasingly inefficient for thicker layers. An exception is an OLED with doped charge transporting layers [30]. However, doping reduces material transparency, making this approach unacceptable for lasers.

Electrically pumped OSL's can be designed employing organic waveguides with contact electrodes on both sides of the organic film, as shown in Fig. 6, similar to a conventional inorganic diode laser. Optical losses in such waveguides composed of thin (100–200 nm) organic films are strongly affected by absorption in the electrodes due to substantial penetration of waveguide modes into the contact layers [15]. The waveguide losses can be considerably reduced if thin transparent ITO contact layers (with optical losses of $\alpha < 300 \text{ cm}^{-1}$ in the 550–750-nm spectral range) are used.

The waveguide OLED's shown in Fig. 6 were fabricated on a (100) Si-SiO₂ substrate consisting of a 100-nm-thick organic film sandwiched between 20-nm-thick ITO contacts. The organic layers were grown in vacuum (5×10^{-7} torr) by sequential deposition of a 500-Å layer of 4, 4'-bis[*N*-(1-naphyl)-*N*-phenyl-amino] bephenyl (α -NPD), 350 Å of Alq₃:DCM, 100 Å of Alq₃, and 50 Å of bathocuproine (BCP) which serves as an electron injecting layer into Alq₃. The ITO layers were radio frequency sputtered at room temperature, with a resistivity of $300 \Omega/\square$. Gold and silver leads were used on the bottom and top ITO contacts, respectively, in order to reduce series resis-

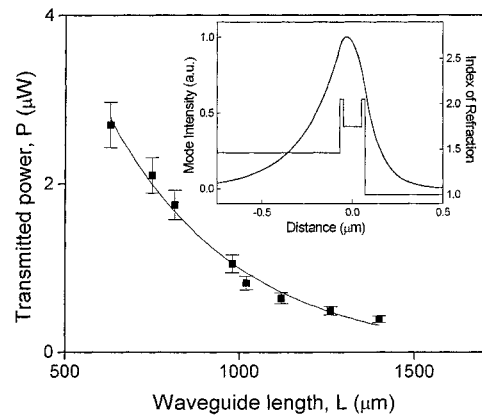


Fig. 7. Laser power transmitted through composite ITO/organic/ITO slab waveguides as a function of the waveguide length. Inset: calculated optical field distribution and refractive index profile in the waveguide shown in Fig. 6.

tance. The OLED's were defined by etching 20- μm -wide by 0.2–1-mm-long openings in the 100-nm-thick SiO₂ insulating layer. The OLED's were cleaved on one side following the fabrication.

The inset in Fig. 7 shows the calculated optical field distribution and refractive index profile in the waveguide. We calculate optical confinement factors of $\Gamma=39\%$ in the organic film and $\Gamma=8\%$, and $\Gamma=5\%$ in the bottom and top ITO layers, respectively. In order to measure the waveguide losses, we also fabricated these structures on a number of 0.6–1.4-mm-wide Si-SiO₂ bars cleaved prior to the deposition of organic films. Coupling a HeNe laser beam ($\lambda=633 \text{ nm}$) into the waveguides and measuring the laser power at the waveguide output, we obtain a waveguide loss of $\alpha=27 \pm 4 \text{ cm}^{-1}$ (see Fig. 7). The estimated optical losses related to light scattering from the ITO surface imperfections are $< 3 \text{ cm}^{-1}$, accounting for an average surface roughness of 1 nm measured using an atomic force microscope. Hence, the losses are primarily due to absorption in ITO which can be further reduced by optimizing the indium-tin ratio and oxygen concentration to achieve maximum transparency while keeping the resistivity sufficiently low [31]. The measured waveguide losses are comparable to mirror losses in an OSL, with optical feedback provided by reflections from the organic film facets. That is, $\alpha = -\ln(R)/L = 32 \text{ cm}^{-1}$, where the facet reflectivity is $R = 7\%$ and the device length is $L = 0.5 \text{ mm}$ [10], making such waveguides feasible for electrically pumped OSL's. The optical feedback may be incorporated by either cleaving the waveguides and using the reflections from the facets, or by employing Bragg reflections from a grating etched in the SiO₂ layer.

The composition of the organic layers was designed to provide for efficient injection of both electrons and holes into the active layer. Metal-free OLED's with ITO contacts to both the electron and hole transporting layers were recently demonstrated [32] employing CuPc as an electron injecting interface layer between the ITO and Alq₃, providing for an ohmic contact. In the waveguide OLED structures, we used BCP instead of CuPc, which also provides for good injection of electrons and is highly transparent in the $\lambda=600\text{--}700\text{-nm}$ spectral range (in contrast to CuPc which is strongly absorbing over those wavelengths). The current-voltage characteristic

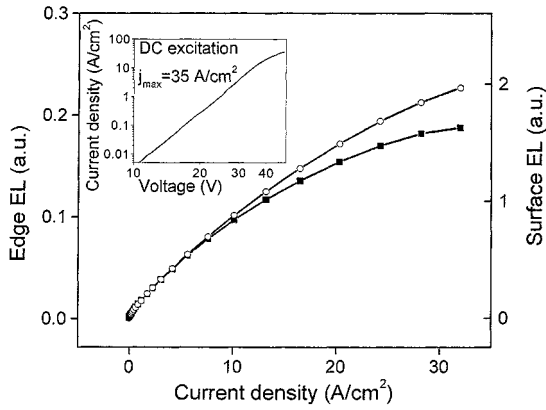


Fig. 8. Electroluminescence measured from the edge (squares) and surface (circles) of a waveguide OLED plotted as a function of current density. Inset: current–voltage characteristic measured for a waveguide OLED.

of the waveguide OLED's is shown in the inset of Fig. 8. A current density of 35 A/cm² is achieved under dc excitation, comparable to currents observed in OLED's with metal Mg–Ag contact to Alq₃.

In Fig. 8, we show the relative electroluminescence emitted from the surface and the edge of the waveguide structures as a function of current density. At high currents, edge emission is less than that from the surface, an effect that is emphasized in Fig. 9, where the emission intensity ratio is plotted as a function of current density. The attenuation of the edge emission may be related to changes in optical transparency of organic materials under current injection. The edge emission propagating through a 200–1000- μ m-long waveguide is more sensitive to such changes, as compared to the surface emission, which passes through less than 0.1 μ m of material.

The edge electroluminescence intensity (I_{edge}) is related to the surface electroluminescence (I_{surf}) via

$$I_{edge} = I_{surf} \cdot \frac{(1 - e^{-(\alpha + \Delta\alpha \cdot \Gamma)L})}{(\alpha + \Delta\alpha \cdot \Gamma)L} \quad (3)$$

where

- L length of the waveguide;
- α waveguide loss;
- $\Delta\alpha$; pump-induced change in the absorption of the organic materials.

The solid line in Fig. 9 shows a fit of the data to (3), assuming that $\Delta\alpha = \xi j$, where ξ is a constant. The best fit was obtained using $\xi = 1.2$ cm/A. The pump-induced absorption should be spectrally broad since no changes in the spectrum of the edge emission were observed at increasing currents (see the inset of Fig. 9). The origin of these effects is discussed below.

V. OPTICAL PROPERTIES OF ORGANIC SEMICONDUCTORS UNDER INTENSE ELECTRICAL EXCITATION

We studied the effects of electrical excitation on the optical properties of Alq₃:DCM2 thin films employing pump and probe spectroscopy [33]. Fig. 10 is a schematic of the experimental setup. The 350- \AA -thick Alq₃:DCM2 films were incorporated into OLED's using 500- \AA -thick α -NPD and 100- \AA -thick Alq₃ as hole and electron transporting layers,

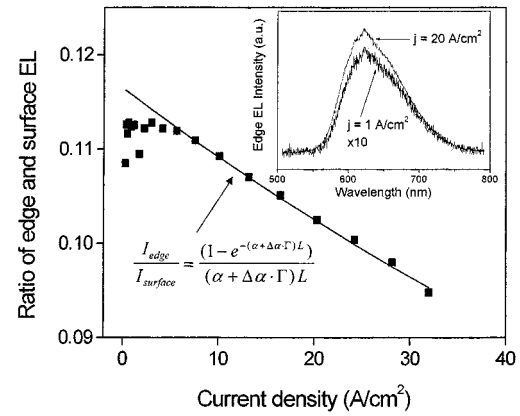


Fig. 9. Ratio between edge and surface electroluminescence of a waveguide OLED as a function of current density. Solid line shows the results of calculations made using the equation shown in the inset and assuming $\Delta\alpha = \xi j$, where j is the current density and $\xi = 1.2$ cm/A. Inset: edge emission spectra measured at different injection currents.

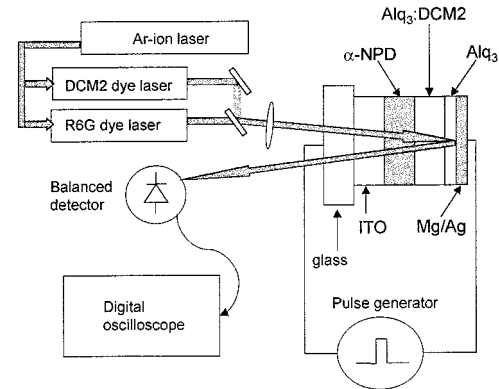


Fig. 10. Experimental setup of the electrooptical pump and probe measurements.

respectively. The structures were fabricated on prepatterned ITO/glass substrates and sealed into a package in an argon ambient. The OLED's were subjected to pulsed ($\tau = 10$ μ s) electrical excitation, and current densities as high as 300 A/cm² were achieved. As an optical probe, we used two tunable dye lasers pumped by an Ar-ion laser. The dye lasers utilized solutions of Rhodamine-6G and DCM2, providing for spectral tunability from 570 to 710 nm. The probe beam was focused on the OLED through the transparent ITO contact and reflected back from the Mg/Ag contact. The probe intensity was measured by a balanced detector placed >1 m away from the OLED in order to minimize the effects of electroluminescence or probe-induced photoluminescence. The detector output was analyzed with a digital oscilloscope, with a total system response time of 1 μ s.

Fig. 11(a) shows spectral dependence of pump-induced changes in absorption of the organic materials calculated from the changes in the probe laser intensity via

$$\Delta I = I_o \cdot (\exp(-\Delta\alpha \cdot 2d) - 1) \quad (4)$$

where I_o is the probe laser intensity and d is the thickness of organic layers. The pump-induced transparency ($\Delta\alpha < 0$) observed between 570–610 nm is due to partial bleaching of Alq₃:DCM2 absorption [see Fig. 11(b)]. However, even

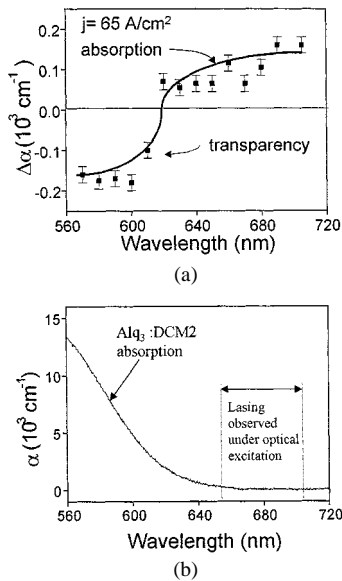


Fig. 11. (a) Spectrum of pump-induced changes in the absorption of $\text{Alq}_3:\text{DCM2}/\alpha\text{-NPD}$ incorporated in an OLED at a current density of $j = 65 \text{ A/cm}^2$. (b) Absorption spectrum of $\text{Alq}_3:\text{DCM2}$, where the DCM2 concentration is 5%.

in the presence of $\Delta\alpha < 0$, the $\text{Alq}_3:\text{DCM2}$ layer remains absorptive since $\Delta\alpha$ is smaller than the total film absorption (i.e., $\alpha + \Delta\alpha > 0$). The pump-induced absorption ($\Delta\alpha > 0$) observed in the spectral range of 620–705 nm, where optical gain was demonstrated in $\text{Alq}_3:\text{DCM2}$ under optical excitation [15], [19], implies the presence of absorbing molecular species formed under carrier injection. In contrast to optical excitation where an electron and a hole in a bound state (or exciton) are formed directly on the same molecule, electrons and holes in electrically pumped OLED's are delivered separately into the active region near the interface between $\alpha\text{-NPD}$ and $\text{Alq}_3:\text{DCM2}$ where they combine to form excitons. As a result, the electron (hole) transporting layer in an OLED contains Alq_3 and DCM2 anions ($\alpha\text{-NPD}$ cations)—molecules with an extra electron (hole). Compared to a neutral molecule, a charged molecule (or polaron) has additional allowed optical transitions leading to so-called polaron absorption. This effect has been studied recently in thin films of conjugated polymers [34], [35] and small molecular weight organic semiconductors [33], [36]. Alternatively, the pump-induced absorption may be due to optical transitions related to triplet excitons also formed under electrical excitation.

Fig. 12 shows the transient response of both the electrical pump as well as the optical probe signals at $\lambda=580 \text{ nm}$ and 680 nm measured at $j = 65 \text{ A/cm}^2$. The decay of induced absorption [see Fig. 12(c)] is nonexponential and has fast and slow decaying components ($\tau=10\text{--}100 \mu\text{s}$), suggesting that observed effects are primarily related to polarons rather than to triplet excitons. We calculate an Alq_3 polaron diffusion coefficient at room temperature of $D_{\text{pol}} = 1.25 \times 10^{-6} \text{ cm}^2/\text{s}$, compared to $D_{\text{ex}} \sim 10^{-3}\text{--}10^{-4} \text{ cm}^2/\text{s}$ [17], using $D = \mu kT/e$, where $\mu = 5 \times 10^{-5} \text{ cm}^2/\text{V}\cdot\text{s}$ is the Alq_3 mobility and e is the electron charge. We then estimate the diffusion time of Alq_3 polarons and excitons through a $500\text{-}\text{\AA}$ -thick film (half of the total Alq_3 layer thickness) of $\tau_{\text{pol}} \sim 10 \mu\text{s}$ and $\tau_{\text{ex}} \sim 10\text{--}100 \text{ ns}$,

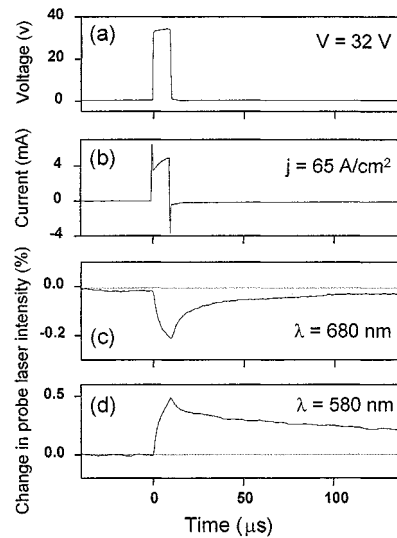


Fig. 12. The transient response of: (a) the voltage applied to the OLED, (b) the current in the OLED, and (c), (d) the probe laser intensity at different wavelengths. Here, positive transients correspond to induced transparency (i.e., $\Delta\alpha < 0$) and negative to induced absorption (i.e., $\Delta\alpha > 0$).

respectively. Since the polaron diffusion time (or lifetime) is an exponential function of its energy with respect to the LUMO, polarons trapped on DCM2 molecules are expected to have even longer lifetimes, contributing to the slowly decaying nonexponential transient response of the OLED. This argument is also supported by the results of the optical pump–probe experiments (Section III), where long decay times of pump-induced absorption were observed in $\text{Alq}_3:\text{DCM}$ films, in contrast to relatively fast decay observed in undoped Alq_3 films.

The decay of pump-induced transparency [see Fig. 12(d)] is also nonexponential. We attribute the initial fast decay to DCM2 singlet excitons which recombine radiatively with $t_{\text{sp}} = 5 \text{ ns}$ (well below our experimental resolution). The slow decay is due to long-lived DCM2 polarons. Polarons may contribute to induced transparency since an extra electron in the LUMO reduces the optical cross section and changes the energy of a highest occupied molecular orbital (HOMO)-LUMO transition due to the Frank–Condon effect [14]. The contribution of the fast decaying (exciton) component to the induced transparency is almost negligible compared to the slowly decaying (polaron) contribution. This originates from the difference in the exciton and polaron lifetimes resulting in a higher concentration of polarons. We estimate the density of Alq_3 polarons as $\rho_p \cong 5 \times 10^{18} \text{ cm}^{-3}$ at $j = 100 \text{ A/cm}^2$. Here, $\rho_p \cong jt_p/ed$, where d is Alq_3 layer thickness (400 \AA). Also, $t_p = d^2/\mu V = 30 \text{ ns}$ is the time of flight of an electron through a $400\text{-}\text{\AA}$ -thick Alq_3 layer at $V = 30 \text{ V}$. In contrast, the density of singlet excitons is $\rho_{\text{ex}} \cong 2 \times 10^{17} \text{ cm}^{-3} < \rho_p$ at $j = 100 \text{ A/cm}^2$, calculated using $\rho_{\text{ex}} \cong jt_{\text{sp}}/4ed$, where $t_{\text{sp}} = 5 \text{ ns}$ is the exciton spontaneous radiative decay time, and the factor of 1/4 approximates the fraction of excitons in radiative singlet states using simple spin statistical arguments.

Both pump-induced transparency and absorption are linear functions of current density (see Fig. 13), as expected for effects related to single charge excitations. The pump-induced transparency measured at $\lambda=570 \text{ nm}$ reaches $\Delta\alpha=-350 \text{ cm}^{-1}$

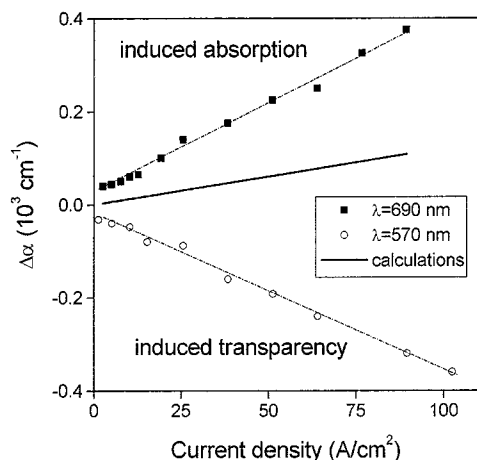


Fig. 13. Dependence of the pump-induced absorption and transparency on current density in $\text{Alq}_3:\text{DCM}_2/\alpha\text{-NPD}$ OLED's. Dashed lines are fits to the experimental points. The solid line shows the pump-induced loss calculated from the electroluminescence response of waveguide OLED's shown in Fig. 6.

at $j = 100 \text{ A/cm}^2$. Nevertheless, $|\Delta\alpha|$ remains well below the absorption of $\alpha = 10^4 \text{ cm}^{-1}$ for $\text{Alq}_3:\text{DCM}_2$ at this wavelength [see Fig. 10(b)], and, therefore, no net optical gain is observed. Current densities as high as 300 A/cm^2 were achieved in the OLED's with an additional 50-\AA -thick layer of CuPc placed between the ITO and $\alpha\text{-NPD}$. However, the pump-induced changes measured for these OLED's are primarily related to polarons formed in CuPc which has a strong absorption in the spectral range of $\lambda=560\text{--}720 \text{ nm}$ [33].

VI. DISCUSSION

The results of pump and probe experiments explain the observed attenuation of the waveguided OLED emission, discussed in Section IV. The DCM2 emission spectrum [see Fig. 1(e)] overlaps primarily with the polaron absorption spectrum rather than with the induced transparency [see Fig. 11(a)]. This leads to effective attenuation of that fraction of electroluminescence coupled to the waveguide modes. The linear dependence of pump-induced absorption calculated from the ratio of surface and edge electroluminescence, shown in Fig. 13 as the solid line, agrees qualitatively with our pump and probe measurements. The quantitative discrepancy (by a factor of 3) may be due to the electroluminescence radiated at small angles to the OLED surface, which is difficult to discern from the waveguided electroluminescence.

These results also provide insight into the origin of induced absorption in $\text{Alq}_3:\text{DCM}$ observed under quasi-CW optical excitation (Section III). As we have shown in Section V, the absorption induced by the electrical current is primarily due to polarons, which are most likely a source of optically induced absorption as well. If the contribution of triplet excitons to the induced absorption were significant, we would expect to see substantially decreased transient decay times observed in the pump and probe experiments (Fig. 12).

From all these experiments, it becomes clear that the OSL waveguide structures can be fabricated using thin organic

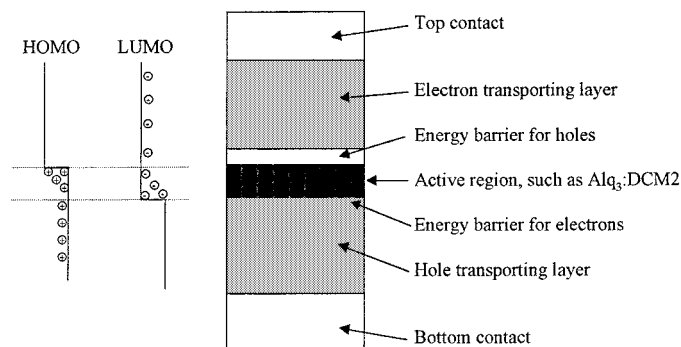


Fig. 14. Schematic of a double-heterostructure OLED with the energy band diagram shown on the left.

films combined with transparent ITO contacts. The excitation levels needed for lasing action to occur ($j \sim 80 \text{ A/cm}^2$) may be achieved in such structures, at least under pulsed excitation. The problem is to deliver this excitation to the laser material without inducing significant absorption in the charge transporting layers. Similar problems exist in inorganic semiconductor lasers, where doping of charge transporting layers leads to optical losses due to free carrier absorption. However, absorption induced by carriers trapped in organic materials is a much stronger effect compared to absorption by free carriers, at least in the visible and near-infrared spectral range. This is due to the higher oscillator strength of molecular transitions and the low charge carrier mobility in organic films, where the transmission of even a modest electrical current requires a high spatial concentration of carriers.

In order to reduce polaron effects, organic double-heterostructures, shown schematically in Fig. 14, can provide the benefit of separating the functions of charge transport and light emission to different materials. The light-emitting layer, composed of $\text{Alq}_3:\text{DCM}_2$, for example, is confined between electron and hole barrier layers. This provides for a high concentration of both electrons and holes (or excitons) in the $\text{Alq}_3:\text{DCM}_2$ layer, leaving the polarons (or single-carrier excitations) in the charge transporting layers. The charge transporting materials are selected according to the spectral characteristics of polarons in these materials in order to minimize the overlap between the charge-induced absorption and the optical gain spectrum. Unfortunately, experimental studies of polaron absorption have thus far been limited to a small number of materials, and theoretical models are not yet capable of accurately predicting the polaron absorption spectra. It is expected, however, that optical properties of polarons strongly depend on the structure of organic molecules, leaving opportunities for suitable materials to be eventually identified. However, finding such materials will require a systematic study of polaron effects in a variety of charge transporting organic films.

Another potential approach to OSL design is to employ Forster energy transfer of excitons between inorganic and organic semiconductors [37]. In such hybrid organic-inorganic systems, the inorganic material can be used for charge transport and the organic material for light emission. In this case, no polarons are induced in the organic material, since excitons are

formed in the inorganic regions of the structure. This type of energy transfer remains, so far, only a theoretical prediction.

In conclusion, we have demonstrated that waveguides composed of thin organic films and ITO electrodes provide for low optical losses ($\alpha=27\pm 4\text{ cm}^{-1}$) and efficient current injection ($j_{\text{max}} = 35\text{ A/cm}^2$), making them feasible for eventual use in thin-film organic semiconductor lasers. The main challenges in realizing OSL's is primarily related to absorption induced by the injection of charge carriers in the organic films. The spectral characteristics of these effects have to be considered in the selection of materials and structures used in OSL's. Induced absorption can be also reduced employing organic double heterostructures or hybrid organic-inorganic systems.

REFERENCES

- [1] P. P. Sorokin and J. R. Lankard, *IBM J. Res. Dev.*, vol. 10, p. 162, 1966.
- [2] B. H. Soffer and B. B. McFarl, *Appl. Phys. Lett.*, vol. 10, p. 266, 1967.
- [3] H. Kogelnik and C. V. Shank, *Appl. Phys. Lett.*, vol. 18, p. 152, 1971.
- [4] N. Karl, *Phys. Stat. Sol. (a)*, vol. 13, p. 651, 1972.
- [5] H. S. Avanesyan, V. A. Benderskii, V. Kh. Brinkenstein, V. L. Broude, and A. G. Lavrushko, *Phys. Stat. Sol. (a)*, vol. 19, p. K121, 1973.
- [6] N. Tessler, G. J. Denton, and R. H. Friend, *Nature (London)*, vol. 382, p. 695, 1996.
- [7] F. Hide, M. A. Diaz-García, B. J. Schwartz, M. R. Andersson, Q. Pei, and A. J. Heeger, *Science*, vol. 273, p. 1833, 1996.
- [8] S. V. Frolov, M. Ozaki, W. Gellermann, Z. V. Vardeny, and K. Yoshino, *J. Appl. Phys.*, vol. 35, p. 1371, 1996.
- [9] H. J. Brouwer, V. V. Krasnikov, A. Hilberer, and G. Hadziioannou, *Adv. Mater.*, vol. 8, p. 935, 1996.
- [10] V. G. Kozlov, V. Bulovic, P. E. Burrows, and S. R. Forrest, *Nature (London)*, vol. 389, p. 362, 1997.
- [11] M. Berggren, A. Dodabalapur, R. E. Slusher, and Z. Bao, *Nature (London)*, vol. 389, p. 466, 1997.
- [12] V. G. Kozlov, V. Bulovic, V. B. Khalfin, and S. R. Forrest, *Appl. Phys. Lett.*, vol. 71, p. 2575, 1997.
- [13] V. Bulovic, V. G. Kozlov, V. B. Khalfin, and S. R. Forrest, *Science*, vol. 279, p. 553, 1998.
- [14] M. Pope and C. E. Swenberg, *Electronic Processes in Organic Crystals*, New York: Oxford University Press, 1982.
- [15] V. G. Kozlov, V. Bulovic, P. E. Burrows, M. Baldo, V. B. Khalfin, G. Parthasarathy, and S. R. Forrest, *J. Appl. Phys.*, vol. 84, p. 4096, 1998.
- [16] C. B. Roxlo and E. Yablonovitch, *Opt. Lett.*, vol. 8, p. 271, 1983.
- [17] C. W. Tang, S. A. VanSlyke, and C. H. Chen, *J. Appl. Phys.*, vol. 65, p. 3610, 1989.
- [18] V. G. Kozlov, P. E. Burrows, G. Parthasarathy, and S. R. Forrest, *Appl. Phys. Lett.*, vol. 74, p. 1057, 1999.
- [19] M. Berggren, A. Dodabalapur, and R. E. Slusher, *Appl. Phys. Lett.*, vol. 71, p. 2230, 1997.
- [20] S. V. Frolov, Z. V. Vardeny, and K. Yoshino, *Appl. Phys. Lett.*, vol. 72, p. 1802, 1998.
- [21] M. Meier, A. Mekis, A. Dodabalapur, A. Timko, R. E. Slusher, J. D. Joannopoulos, and O. Nalamasu, *Appl. Phys. Lett.*, vol. 74, p. 7, 1999.
- [22] S. Y. Chou, P. Krauss, and P. J. Renstrom, *Science*, vol. 272, p. 85, 1996.
- [23] S. Y. Chou, P. Krauss, W. Zhang, L. Guo, and L. Zhuang, *J. Vac. Sci. Technol.*, vol. B15, p. 2897, 1997.
- [24] P. E. Burrows, Z. Shen, V. Bulovic, D. M. McCarty, S. R. Forrest, J. A. Cronin, and M. E. Thompson, *J. Appl. Phys.*, vol. 79, p. 7991, 1996.
- [25] S. A. Kovalenko, N. P. Ernsting, and J. Ruthmann, *Chem. Phys. Lett.*, vol. 258, p. 445, 1996.
- [26] A. F. Mills, *Heat Transfer*. Concord: Irwin, 1992.
- [27] F. J. Duarte and L. W. Hillman, *Dye Laser Principles*. San Diego, CA: Academic, 1990.
- [28] M. Klessinger and J. Michl, *Excited States and Photochemistry of Organic Molecules*, New York: VCH Publishers, 1994.
- [29] P. E. Burrows, V. Bulovic, S. R. Forrest, L. S. Sapochak, D. M. McCarty, and M. E. Thompson, *Appl. Phys. Lett.*, vol. 65, p. 2922, 1994.
- [30] A. Yamamori, C. Adachi, T. Koyama, and Y. Taniguchi, *Appl. Phys. Lett.*, vol. 72, p. 2147, 1998.
- [31] K. L. Chopra, S. Major, and D. K. Pandya, *Thin Solid Films*, vol. 102, pp. 1-46, 1983.
- [32] G. Parthasarathy, P. E. Burrows, V. B. Khalfin, V. G. Kozlov, and S. R. Forrest, *Appl. Phys. Lett.*, vol. 72, p. 2138, 1998.
- [33] V. G. Kozlov, P. E. Burrows, G. Parthasarathy, and S. R. Forrest, *Appl. Phys. Lett.*, vol. 74, p. 1057, 1999.
- [34] M. Tessler, N. T. Harrison, and R. H. Friend, *Adv. Mater.*, vol. 10, p. 64, 1998.
- [35] S. V. Frolov, W. Gellermann, Z. V. Vardeny, M. Ozaki, and K. Yoshino, *Synthetic Metals*, vol. 84, p. 493, 1997.
- [36] G. Lanzani, S. Frolov, M. Nisoli, P. A. Lane, S. De Silvestri, R. Tubino, F. Abbate, and Z. V. Vardeny, *Synthetic Metals*, vol. 84, p. 517, 1997.
- [37] V. M. Agranovich and D. M. Basko, unpublished.

V. G. Kozlov, photograph and biography not available at the time of publication.

G. Parthasarathy, photograph and biography not available at the time of publication.

Paul E. Burrows received the Ph.D. degree in physics from Queen Mary College, London, U.K.

After post-doctoral appointments at the Riken Institute in Japan and the University of Southern California, where he developed ultrahigh vacuum deposition techniques for producing highly ordered thin films of organic molecules, he joined the Princeton University Center for Optoelectronic Materials (POEM), Princeton University, Princeton, NJ, and was appointed to the permanent post of Research Scholar in 1995. His current research involves study of the growth and structure of thin films of small-molecule organic semiconductors, their non-linear optical and electronic properties, and their application in optoelectronic devices, particularly organic light-emitting diodes for full-color flat panel displays. He has co-authored more than 60 papers in scientific journals, including two book chapters and several invited reviews, and holds ten U.S. patents.

Dr. Burrows currently chairs the Technical Subcommittee on Displays of the IEEE Lasers and Electro-Optics Society (LEOS).

V. B. Khalfin, photograph and biography not available at the time of publication.

J. Wang, photograph and biography not available at the time of publication.

S. Y. Chou, photograph and biography not available at the time of publication.

S. R. Forrest, photograph and biography not available at the time of publication.